Gel Formation and Interpolymer Alkyl Chain Interactions with Poly(9,9-dioctylfluorene-2,7-diyl) (PFO) in Toluene Solution: Results from NMR, SANS, DFT, and Semiempirical Calculations and Their Implications for PFO β-Phase Formation

Licínia L. G. Justino,*[,†,‡] M. Luísa Ramos,[†,‡] Matti Knaapila,*[,§] Ana T. Marques,[†,⊥] Christof J. Kudla,[⊥] Ullrich Scherf,[⊥] László Almásy,[∥,○,◆] Ralf Schweins,[#] Hugh D. Burrows,[†] and Andrew P. Monkman[▽]

[†]*Departamento de Química, Faculdade de Ciências e Tecnologia, Universidade de Coimbra, 3004-535 Coimbra, Portugal,* [‡]*Centro de Neurociências e Biologia Celular, Universidade de Coimbra, 3004-517 Coimbra, Portugal,* [§]*Physics Department, Institute for Energy Technology, NO-2027 Kjeller, Norway,* [⊥]*Makromolekulare Chemie, Bergische Universität Wuppertal, D-42097 Wuppertal, Germany,* [∥]*Laboratory for Neutron Scattering, PSI, CH-5232 Villigen, Switzerland,* [○]*Adolphe Merkle Institut, University of Fribourg, CH-1700 Fribourg, Switzerland,* [◆]*Research Institute for Solid State Physics and Optics, Budapest-1525, Hungary,* [#]*Institut Laue-Langevin, DS/LSS Group, 6 Rue Jules Horowitz, F-38042 Grenoble CEDEX 9, France, and* [▽]*OEM Research Group, Department of Physics, Durham University, Durham DH1 3LE, U.K*

ABSTRACT: Interactions between polymer chains of poly(9,9-dioctylfluorene-2,7-diyl) (PF8) have been studied in toluene solution over a wide concentration range using multinuclear NMR spectral and relaxation measurements with both the fully protonated and alkyl chain deuterated polymers, small angle neutron scattering (SANS), together with theoretical calculations using DFT and semiempirical methodologies. Full assignment of the ^{1}H and ^{13}C chemical shifts in the NMR spectra of isolated chains of PF8 has been made using DFT, and are in good agreement with spectra in chloroform and in toluene solutions. Somewhat different behavior is seen in toluene solution, where, upon increasing polymer concentration, broadening of the alkyl chain resonances is seen, consistent with interactions between the side chains. Similar behavior is seen with the ^{2}H resonance of PF8-d_{34}. In both cases, line-narrowing and restoration of the structured alkyl chain resonances is seen upon studying the spectra of concentrated solutions using the magic angle spinning (MAS) technique, in agreement with the attribution of the broadening to interchain interactions between the octyl groups. Support for this interpretation comes from ^{1}H and ^{13}C spin−lattice relaxation time measurements, which also show differences in group dynamics along the alkyl chains. Semiempirical theoretical calculations, using PM3 and PM6 Hamiltonians, add further support to the importance of interactions between the alkyl groups of separate PF8 chains. SANS measurements on PF8 in toluene solutions from very dilute to concentrated solutions, extended to ultrasmall q ranges, provide further insight. Three concentration ranges can be identified. In dilute solutions, the results suggest that PF8 is present as fully dissolved polymer coils. Upon increasing polymer concentration, an intermediate region is observed, in which there are indications of transient contacts between the polymers, which the NMR results suggest involves side chain interactions. As a consequence of interactions between the chains, gel formation occurs. On the basis of these and previous results, some general considerations are presented upon the solubility and aggregation behavior of PF8, including indications of how interactions between alkyl chains may be important in the stabilization of the so-called β-phase of PF8.

I. Introduction

Conjugated polymers (CP) are technologically important materials in the rapidly developing area of organic semiconductors. One major advantage they possess over small molecule organic systems is the possibility of using low-cost solvent-based methodologies, such as inkjet printing,[1] for preparation of thin film optoelectronic devices. This allows large-scale production of flexible systems using reel-to-reel methodologies.[2] However, the luminescence efficiency, charge transport and other properties of these devices are strongly dependent on film morphology, and it is important to be able to both understand and control the characteristics of thin films produced through such processes. There are strong indications that the properties of solution deposited films are closely related to the structures and aggregation characteristics of the polymers in the solutions used for processing.[3−5] We will address one such case.

Polyfluorenes are a particularly important CP family,[6−10] and have excellent photophysical and optoelectronic characteristics.[11] In addition, they show good solubility in many common solvents, and possess an interesting phase behavior,[12] which can lead to different morphologies and characteristics of deposited films depending on molecular weight,[13] side chain length,[14,15] and branching.[14−17] Particularly interesting behavior is observed when films of poly(9,9-dioctylfluorene) (PF8),[18,19] and some other linear side chain poly(9,9-dialkylfluorenes),[20] are obtained from poor solvents. With certain alkyl chain lengths, the so-called β-phase is formed,

*Corresponding authors. (L.L.G.J.) Telephone: +351-239-854453. Fax: +351-239-827703. E-mail: liciniaj@ci.uc.pt. (M.K.) Telephone: +47-6380-6081. Fax: +47-6381-0920. E-mail: matti.knaapila@ife.no.

which shows enhanced emission in light emitting devices, in addition to increased structuring and a red shift in the photoluminescence. This is associated with conformational ordering and formation of a particularly extended chain structure.[8] This can also be induced by addition of various alkyl compounds[21] or phospholipids.[22] However, it is still not clear whether β-phase formation is a precursor to or a consequence of aggregation in solution,[23,24] and there is a clear need for more information on the nature of any supramolecular structures present. Although our knowledge of structures and aggregates in solutions of conjugated polymers is still rather limited, considerable advances have recently been made and valuable data obtained with polyfluorene systems using small-angle X-ray (SAXS)[25−27] and neutron scattering (SANS),[25,26,28−34] light scattering,[27,28,34,36−38] NMR spectroscopy,[31−33,35,39] near-field scanning optical microscopy[40] and atomic force microscopy (AFM).[17,40,41] However, there are still no clear guidelines as to the driving forces which determine the type of aggregate formed. In this work we concentrate on one case involving the important system of polymer gels with spatial inhomogeneity,[42] a materials class which can be readily studied by small-angle scattering techniques.[43] A combination of NMR and small-angle neutron scattering is used. These techniques have been shown in previous studies to provide complementary information about these systems on different length scales.[31−33] We consider the PF8/toluene system, where solution structures have been studied over a wide concentration using a variety of techniques[28,30,31,33,35,37,40,41,44,45] and where gels are formed in dense solutions.[31,37] Results are also presented of DFT and semiempirical calculations, which permit complete assignment of the NMR spectra and also provide insights on interchain association. Finally, aspects of the nature of solvents which favor particular types of aggregation with this class of hairy-rod polymers are addressed.

II. Experimental Section

Materials and Sample Preparation. Poly[9,9-di(*n*-octyl-d_{17})-fluorene-2,7-diyl] (PF8-d_{34}) with number-averaged molecular weight (M_n) of 73.1 kg/mol and weight-averaged molecular weight (M_w) o f 144 kg/mol was prepared following the microwave-assisted Yamamoto-type polymerization with $Ni(COD)_2$ as catalyst and 2,7-dibromo-9,9-dioctylfluorene monomer containing octyl-d_{17} side chains, as described previously.[8,30,46]

For NMR experiments, poly(9,9-di-*n*-octylfluorene-2,7-diyl) (PF8) was obtained from Aldrich (M_n = 15.8 kg/mol, M_w = 58.2 kg/mol). Alkyl chain deuterated and nondeuterated PF8 samples were prepared by dissolving weighed amounts of the polymers in chloroform-*d* supplied by Sigma-Aldrich (99.8% D) or toluene-d_8 (99% D). Complete dissolution of the polymers at the 2.5% and 6% (i.e., 25−60 mg/mL) concentrations was achieved by warming the samples in a water bath. The samples were kept protected from light.

For neutron scattering, PF8 (M_n = 47 kg/mol, M_w = 153 kg/mol) was mixed to deuterated toluene (toluene-d_8) that was supplied by Sigma-Aldrich (99.6% D, for low concentration samples (≤2 mg/mL)) or Armar Chemicals, Swizerland (99.5% D, high concentration samples (≥5 mg/mL)). The neutron scattering length density of PF8 is 0.702×10^{10} cm^{-2} and that of toluene-d_8 is 5.662×10^{10} cm^{-2}. The molecular weight is larger than the one of the sample studied by NMR. However, the fact that similar NMR spectral behavior was observed with this and the PF8-d_{34}, which has a comparable molecular weight to the PF8 sample used in SANS, suggests that the NMR experiments are relatively insensitive to the polymer size (vide infra).

NMR. ^{1}H, ^{2}H, and ^{13}C NMR spectra were recorded on a Varian VNMRS 600 MHz spectrometer, at 599.72, 92.06, and 150.80 MHz, respectively. The magic angle spinning (MAS) spectra were obtained using a PFG nano gHX probe at a spinning speed of 4 kHz in a 4 mm rotor. The spin−lattice relaxation times (T_1) were measured using the inversion−recovery pulse sequence, schematically represented as d_1−180°−d_2 −90°−T_a, with $d_1 + T_a \geq 5T_{1,max}$. The signals of $CDCl_3$ at δ = 7.27 ppm and of toluene at δ = 2.09 ppm, relative to TMS, were used as internal references for ^{2}H and ^{1}H, while the ^{13}C triplet of $CDCl_3$ centered at δ = 77.23 ppm and the heptet of toluene centered at δ = 20.40 ppm were used as internal references for ^{13}C. All NMR measurements were carried out at 25 °C.

Small Angle Neutron Scattering (SANS). SANS measurements of the low-concentration samples (0.2−2 mg/mL) were carried out at the LOQ beamline at ISIS Facility, Rutherford Appleton Laboratory (U.K.).[47] The LOQ instrument at ISIS uses incident wavelengths between 2.2 and 10 Å sorted by time-of-flight with a sample-to-detector distance of 4.1 m resulting in a q range between 0.006 and 0.24 Å^{-1}. The samples were in quartz cuvettes (Hellma) of 2 mm path length placed in a thermostat and kept at 25.0 ± 0.5 °C during measurements. The raw data were corrected for the transmission, D_2O background, sample cell, and detector efficiency. The 2D scattering patterns were azimuthally averaged and converted to an absolute scale. The data for each sample was collected for 1 h.

SANS measurements of the intermediate- (5−10 mg/mL) and high-concentration samples (30−70 mg/mL) were performed at the instrument D11 at the Institut Laue-Langevin (ILL, France). Scattering intensities were measured with a two-dimensional position-sensitive ^{3}He detector with an array of 128 × 128 cells of 7.5 mm ×7.5 mm size. The measurements were done using two wavelengths in order to cover a large q range. Instrument settings were as follows: a wavelength of 6 Å with sample-to-detector distances of 1.5 m, 8 and 34 m; and a wavelength of 16.5 Å with a sample-to-detector distance of 34 m. These settings provide a q range of 0.00058−0.4 Å^{-1}. All samples and backgrounds were confined in rectangular 1 mm Hellma cells of type 404−QS. The cells were placed in a high-precision temperature-controlled copper rack; measurements were performed at 25 °C. The two-dimensional scattering data obtained were radially averaged and background-corrected using the ILL standard data reduction routines. H_2O was used as secondary standard (calibrated against monodisperse polymer standards). Data were put on an absolute scale by using the known wavelength-dependent effective cross section of H_2O, determined for D11 with its current ^{3}He detector to $(d\Sigma/d\Omega)_{H_2O}$ = 0.983 cm^{-1} at 6 Å and 1.843 cm^{-1} at 16.5 Å. The incoherent background from hydrogen-containing polymer was taken into account by adding a corresponding amount of toluene to toluene-d_8 and using scattering of this mixture for background subtraction.

The scattering curves were interpreted using scaling concepts by considering scattering intensity $I(q) \sim q^{-\alpha}$. PF8 is known to be a rodlike polymer in toluene solutions.[30] When the curves show a crossover point from rodlike behavior ($\alpha \approx 1$) at $q \approx q^*$, the persistence length of the polymer, l_p, was estimated from the relation $q^* l_p \approx 1.9$. For the intermediate solutions (5−10 mg/mL) this simple interpretation was enhanced by estimating the phenomenological scatterer size using the indirect Fourier transformation program GNOM.[48] For the concentrated solutions (30−70 mg/mL), the subsequent fit of the scattering factors was adapted from Chen and co-workers[31] In this procedure, the material was expected to act as a dynamic mesh of long rodlike polymers joined together via overlapping nodes. A two-component model was employed to fit the entire scattering curve. The low q part of the curve was fitted to the Debye−Bueche equation

$$I(q) \sim \frac{1}{(1 + \xi_s^2 q^2)^2} \quad (1)$$

where ξ_s is the correlation length connected to the average distance between aggregate domains. The high-q part was fitted to an Ornstein−Zernike type equation

$$I(q) \sim \frac{1}{1 + \xi_d q \exp(q^2 R^2/4)} \quad (2)$$

where ξ_d represents the mesh size of the dynamic network and R is the radius of the rodlike polymer.

III. Computational Section

The geometry optimization of the PF8 monomer was performed by DFT without symmetry constraints using the GAMESS[49] code. The calculation employed the B3LYP (Becke three-parameter Lee−Yang−Parr exchange correlation functional, which combines the hybrid exchange functional of Becke,[50] with the correlation functional of Lee, Yang and Parr (LYP)[51]) and the 6-31G(d,p) basis sets for the expansion of the Kohn−Sham orbitals. At the final equilibrium geometry with minimum energy the gradient was 1×10^{-05} hartree bohr^{-1}. For the optimized structure the nuclear shieldings were computed using the NWCHEM[52] program at the B3LYP/GIAO (gauge-including atomic orbital method) level. The 6-31G(d,p) basis sets and a fine integration grid (FINE option) were used. ^{13}C and ^{1}H relative chemical shifts (δ) are given with respect to the absolute shielding values (σ) of tetramethylsilane (TMS) obtained at the same computational level ($\delta = \sigma_{ref} - \sigma$).

The aggregation behavior of PF8 was simulated using semiempirical quantum chemistry calculations for a system composed of two PF8 trimers placed with a distance of 21.5 Å separating the plans of the backbones. The system was optimized in vacuum using the PM3 and the PM6[53] Hamiltonians and the EF routine implemented in the MOPAC2007[54] system of programs. At the final equilibrium geometry, the gradient was 0.01 kcal mol^{-1} Å^{-1}.

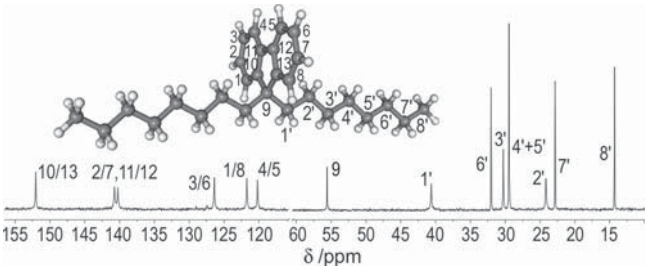

Figure 1. ^{13}C NMR spectrum of a 6% (60 mg/mL) PF8 solution in $CDCl_3$ at 25 °C. Inset: B3LYP/6-31G(d,p) optimized geometry of the PF8 monomer. Note the separate numbering of the backbone and side-chain atoms.

IV. Results and Discussion

NMR Studies on Nondeuterated PF8. Figure 1 shows a ^{13}C NMR spectrum of a 6% (or 60 mg/mL) PF8 solution in chloroform. As with our previous work with poly(9,9-bis(2-ethylhexyl)fluorene-2,7-diyl) (PF2/6),[39] in this solvent the polymer is considered to be dissolved at the molecular level to give isolated polymer chains. The assignment of the resonances was accomplished by computing, at the DFT/GIAO level, the NMR chemical shifts for the DFT-optimized geometry of the monomer. The computed values are compared in Table 1 with the experimental shifts for the polymer in chloroform and in toluene solutions. The only feature which is worthy of note is that the (4′ + 5′) resonance of the chloroform spectrum is split into two separate resonances in the toluene spectrum, with the chemical shifts indicated in Table 1.

The alkyl regions of the ^{1}H spectra in toluene and in chloroform of the same sample (Figure 2) also show some differences. The CH_2 protons 2′ to 7′ give rise to just two separate bands in chloroform, spanning the region from 1.18 to 1.25 ppm (0.07 ppm), but they present three distinct bands in toluene, ranging from 1.00 to 1.21 ppm (0.21 ppm). This result suggests much more rigid conformations for the alkyl chains of the polymer in toluene, in agreement with this solvent's poorer solubilizing properties for PF8, which will permit stronger interactions between the polymer chains. The ^{1}H assignment of the resonances was based on the computed values for the monomer, also presented in Table 1. Our assignment is in accordance with that given by Leclerc et al.[55] for the ^{13}C aromatic resonances of a low-molecular-weight PF8 in $CDCl_3$, for which spectra similar to the present ones were observed.

To analyze the dynamics of PF8 in concentrated solutions in a good solvent, where we expect very few polymer−polymer interactions, and in a poorer solvent, in which we expect some aggregation to occur, we have measured the spin−lattice relaxation times of the ^{1}H and ^{13}C atoms of the alkyl chains of PF8 in 6% solutions in chloroform and in toluene. The NMR δ and J values are interpreted in terms of the structure of each molecule, and the relaxation times T_1 and T_2 (spin−lattice and spin−spin relaxation) are affected by macroscopic dynamical properties of the nuclear

Table 1. Calculated NMR Chemical shifts for the PF8Monomer in Vacuum (B3LYP/6-31G(d,p)//B3LYP/6-31G(d,p)[a]) and Experimental Chemical Shifts (ppm) of the PF8 Polymer in $CDCl_3$

Site	$\delta(^{13}C_{calc.})$	$\delta(^{13}C_{expt.})$	$\delta(^{1}H_{calc.})$	$\delta(^{1}H_{expt.})$
		Quaternary C		
$C_{(10)}/C_{(13)}$	147.94	152.04	-	-
$C_{(11)}/C_{(12)}$	139.88	140.73 and	-	-
$C_{(2)}/C_{(7)}$	b	140.25	-	-
$C_{(9)}$	58.89	55.58	-	-
		Aromatic CH		
$C_{(3)}H/C_{(6)}H$	122.94	126.38	b	7.73; 7.71(d)[c]
$C_{(1)}H/C_{(8)}H$	117.87	121.72	b	7.71
$C_{(4)}H/C_{(5)}H$	115.46	120.18	7.84	7.88; 7.87(d)
		Alkylic region		
$C_{(1')}H_2$	45.08	40.62	2.46	2.16(b)[c]
$C_{(2')}H_2$	26.12	24.16	1.05	
$C_{(3')}H_2$	33.92	30.27	1.38	
$C_{(4')}H_2$	33.60	29.45[d]	1.22	1.25-1.18
$C_{(5')}H_2$	34.17	*29.70 and 29.62*[e]	1.34	*1.21-1.00*
$C_{(6')}H_2$	34.83	32.03	1.26	
$C_{(7')}H_2$	26.42	22.83	1.12	
$C_{(8')}H_2$	15.88	14.29	0.52	0.85

[a] The notation indicates "level of geometry calculation//level of NMR chemical shifts calculation". [b] In the PF8 polymer the 2 and 7 carbons are bonded to the adjacent monomer units, thus the calculated chemical shifts for the monomer at these positions are not suitable for comparison with the experimental shifts. [c] "d" stands for doublet and "b" stands for broad. [d] In chloroform solution, $C_{(4')}$ and $C_{(5')}$ are superimposed. [e] Chemical shifts in toluene are indicated in italics.

Table 2. ^{1}H and ^{13}C Spin−Lattice Relaxation Times Measured for the Alkylic Chains of PF8 6% (60 mg/mL) Solutions in Chloroform and in Toluene at 25 °C

	T_1 (^{1}H) /s		T_1 (^{13}C) /s	
atom	$CDCl_3$	toluene	$CDCl_3$	toluene
$C_{(1')}H_2$	0.87±0.02	0.81± 0.01	0.24±0.01	0.20±0.01
$C_{(2')}H_2$	1.19[a]	1.11[a]	0.29±0.01	0.25±0.01
$C_{(3')}H_2$			0.41±0.01	0.40±0.01
$C_{(4')}H_2$	*(1.34; 1.32; 1.25; 0.86)*	*(1.30; 1.30; 1.26; 0.90; 0.78)*	0.83[b]±0.01	0.77[a] *(0.63; 0.90)*
$C_{(5')}H_2$				
$C_{(6')}H_2$			1.60±0.02	1.44±0.08
$C_{(7')}H_2$			2.37±0.02	2.17±0.11
$C_{(8')}H_3$	1.76±0.12	1.59±0.05	3.24±0.04	3.00±0.16

[a] Average value with estimated error of 5%. [b] In chloroform solution $C_{(4')}$ and $C_{(5')}$ are superimposed.

environment. The nuclear relaxation depends on the existence of molecular motion. This generates fluctuating magnetic fields, which provide a mechanism for the loss of energy from the excited nuclear spins to the surrounding lattice. Thus, the experimental relaxation times can give valuable information on the dynamical properties both of the molecules under study and their interactions with adjacent species.[56,57] For large organic molecules having only carbon and hydrogen atoms ($I = 1/2$), dipolar relaxation is the dominant mechanism. With ^{13}C, where dipolar interactions with the directly bonded ^{1}H spins are dominant, its rate is given by eq 3, which assumes isotropic rotational diffusion of a rigid spheroid molecule:

$$T_1^{-1}(DD) = \frac{1}{10}(2\pi R)^2\tau_c\left[\frac{1}{1+(\omega_X-\omega_A)^2\tau_c^2}+\frac{3}{1+\omega_A^2\tau_c^2}+\frac{6}{1+(\omega_X+\omega_A)^2\tau_c^2}\right] \quad (3)$$

where ω is the Larmor frequency and τ_c is the correlation time, a measure of how rapidly the molecule undergoes reorientation in solution.[56] τ_c is defined as

$$\tau_c = 4\pi\eta a^3/3kT \quad (4)$$

where a is the molecular radius of a molecule, taken as a first approximation to be spherical and η is the viscosity of the medium. R is the dipolar coupling constant:

$$R = (\mu_0/4\pi)\gamma_A\gamma_X(h/4\pi^2)r_{AX}^{-3} \quad (5)$$

in which γ is the magnetogyric ratio. For relatively fast isotropic rotational motions, that is, $\omega\tau_c < 1$ (this means $\tau_c < 10^{-09}s$ for $\nu = 150.8$ MHz), $T_1^{-1}(DD)$ becomes independent of the frequency. This is termed the *extreme narrowing* condition (so-called because T_1 and T_2 become equal) and the relaxation times are given by:

$$T_1^{-1}(DD)(hetero) = T_2^{-1}(DD)(hetero) = \left(\frac{\mu_0}{4\pi}\right)^2\gamma_A^2\gamma_X^2h^2\tau_c/4\pi^2r_{AX}^6 \quad (6)$$

When there are a large number of spin pairs to be considered, the above equations must be modified to take into account the sum of all the interactions with the spin of interest.

Treatment of relaxation in polymers is further complicated[58] by the existence of multiple processes. Although formalisms[59] have been developed for the analysis of relaxation times in macromolecules, where fast internal motions are superimposed on an anisotropic overall motion, this mathematical treatment is beyond the scope of this article and for a qualitative analysis of the T_1 results with ^{13}C we will assume

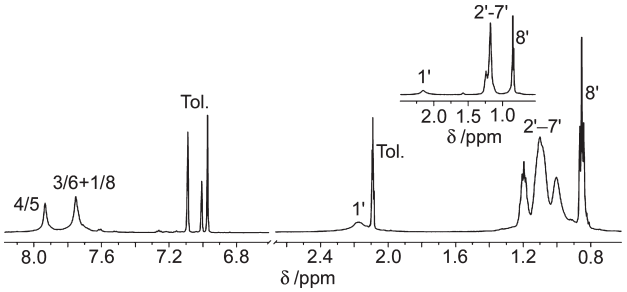

Figure 2. ^{1}H NMR spectrum of a 6% (60 mg/mL) PF8 solution in toluene at 25 °C. Inset: alkyl region of the ^{1}H NMR spectrum of the same sample in $CDCl_3$; (numbering is as defined in Figure 1).

that eqs 3 and 6, which were derived under the assumption of isotropic rotational motion of a spheroid molecule, are valid. We will also assume that the segmental motions in our systems meet the *extreme narrowing* condition, where T_1 is independent of the frequency, and we present in Table 2 the absolute ^{13}C T_1 values for the alkyl chains of PF8 in chloroform and in toluene. Results were also obtained for ^{1}H, but the treatment of the relaxation mechanism is more complicated, since for each proton there are many intramolecular and intermolecular interactions contributing to the ^{1}H T_1 values. Therefore, the ^{1}H results are only given for comparison, and no detailed analysis is attempted.

In both solvents, the ^{13}C T_1 values increase from $C_{(1')}$, to $C_{(8')}$, along the polymer alkyl chain. This is a consequence of the increasing flexibility on going from the methylene group linked to the fluorene to the terminal methyl group, and is explained in terms of the different individual correlation times for the successive internal motions in the chain, in addition to the correlation time, τ_c, defined for the overall molecular motion. A second important observation is that all the ^{13}C T_1 values decrease on going from chloroform to toluene solution, and that the T_1 values of the carbons of the end of the chain, $C_{(6')}$ and $C_{(7')}$ (the contributions to the T_1 values of $C_{(8')}$ will be discussed below), are those most affected with the change in solvent. The smaller T_1 values in toluene (in the *extreme narrowing* condition,$\omega\tau_c < 1$) indicate, through eq 6, longer correlation times in this solvent, showing a decrease in the mobility of the alkyl chains. This suggests stronger polymer−polymer interactions in toluene, conferring certain rigidity to the alkyl chains. These are expected to lead to some overlap (or interdigitation) of the alkyl chains, explaining the larger effect seen for the $C_{(6')}$ and $C_{(7')}$ carbons. Although $C_{(8')}$ is the carbon atom most markedly affected, this belongs to a methyl group, and in addition to having a different number of H atoms directly connected to it (which would decrease its $T_1(DD)$ compared to the CH_2 carbons), the spin-rotation relaxation mechanism also contributes to, and probably dominates, its relaxation. With the ^{1}H T_1 values, although, as mentioned, they are affected by

intermolecular contributions to their relaxation, they show a similar evolution on going along the polymer alkyl chains and on changing the solvent.

When handling the solutions, the 6% PF8/toluene solution was observed to be more viscous than the 6% PF8/chloroform solution, in agreement with the occurrence of stronger polymer−polymer interactions. Future rheological studies will be directed to relate viscosity with solution structure. A higher viscosity, through eq 4, at constant temperature, indicates longer τ_c values for PF8 in toluene, in agreement with the assumption that our systems meet the $\omega\tau_c < 1$ condition (for $\omega\tau_c = 1$, T_1 reaches a minimum and for $\omega\tau_c > 1$, T_1 increases with τ_c[56]). As noted above, in such systems which are very far from a spheroid geometry, we must distinguish the slow overall motion involving the PF8 backbone from the fast intramolecular motions in the alkyl lateral chains. As discussed elsewhere,[56−58,60] the processes seen in T_1 measurements in the megahertz region correspond to relaxation by fast motions such as alkyl chain segmental fluctuations.

Since the spectral line-widths at half-height can be related to the spin−spin relaxation time through equation

$$\Delta\nu_{1/2} = 1/\pi T_2^* \qquad (7)$$

the small values for T_1 (which is equal to T_2 in the conditions assumed for eq 6) of carbons $C_{(1')}$, $C_{(2')}$, and $C_{(3')}$ and protons $C_{(1')}H_2$ explain the larger widths of the observed signals for these atoms. T_2^* is the effective T_2 obtained from the observed line-width, which is likely to have a contribution from the inhomogeneity of the applied magnetic field. The T_2^* values were determined for the alkyl carbon atoms of PF8 in $CDCl_3$ from the spectral line-widths, and the values are compatible with the experimental T_1 values. For example, for the $C_{(6')}$, T_2^* is 0.27 s and T_1 is 1.60 s. However, we must note that the differences between the experimental values of T_2^* and T_1 in this system can also have a contribution from the fact that the model of isotropic rotation may not be totally appropriate to these motions.

Polymer−polymer interactions in PF8 were also simulated using semiempirical calculations. A system of two F8 trimers was considered in vacuum and the input was built so that the distance between the planes of the backbones was approximately 21.5 Å. The geometry was optimized using the PM3 and the PM6 Hamiltonians and the PM3 structure is shown in Figure 3. The distance between the planes of the backbones decreased to approximately 18.5 Å, which can be attributed to the existence of van der Waals attraction between the alkyl chains. The optimized geometry shows some interdigitation of the chains. The PM6 structure shows an even higher degree of interaction and proximity between the chains, although PM6 is known to suffer from overestimation of nonbonding interactions in some molecular systems.[54] The PM6 results agree with PM3 in showing a strong tendency of PF8 to aggregate through interdigitation of the alkylic chains. This is in perfect accord with the occurrence of major changes in the above experimental T_1 values of the $C_{(6')}$ and $C_{(7')}$ carbons.

Studies on the Deuterated Polymer PF8-d_{34}. The ^{1}H NMR spectra of alkyl chain deuterated PF8 are shown in Figure 4 for a range of concentrations from 0.7% to 6% (or 7−60 mg/mL) (only the alkyl region is shown). A high-resolution magic angle spinning (MAS) spectrum is also shown for the more concentrated solution. The 0.7% solution spectrum shows the residual ^{1}H resonances of the deuterated polymer coupled with the deuterium nuclei. The relative intensities of the resonances are affected by the presence of defects from the deuteration of the individual sites. The ^{1}H spectra of the

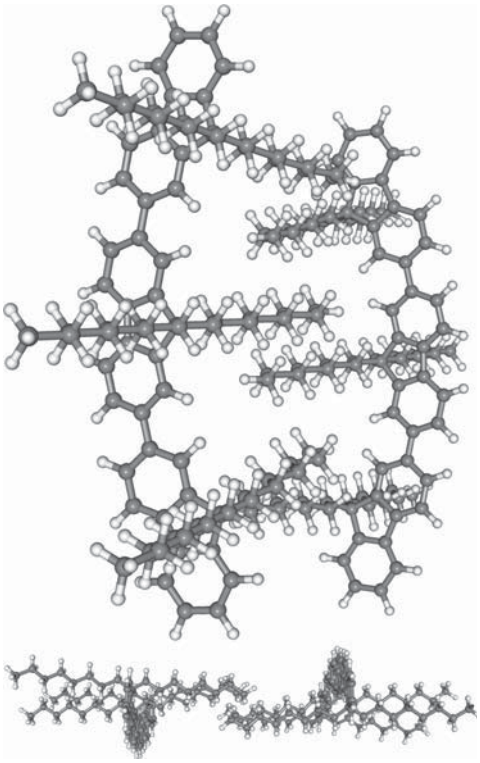

Figure 3. Two perspectives of the PM3 optimized geometry of an aggregate of two F8 trimers in vacuum.

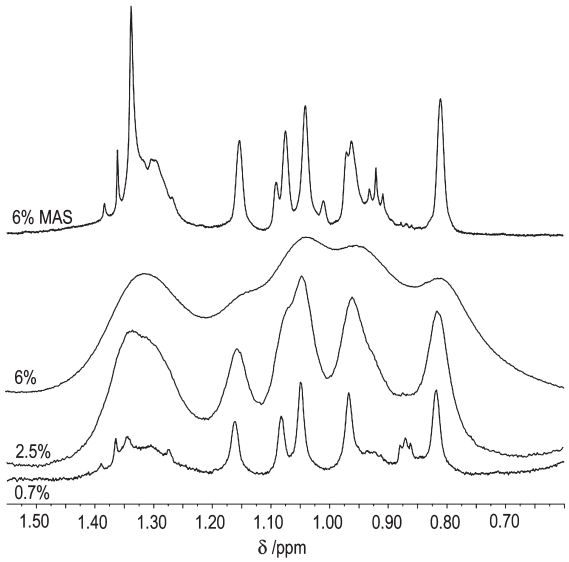

Figure 4. ^{1}H NMR spectra of residual protons of PF8-d_{34} solutions in toluene at indicated concentrations; the 6% MAS spectrum was acquired at 4 kHz spinning rate.

2.5% and 6% solutions show the same resonances as the 0.7% solution, but they are strongly broadened due to residual magnetic dipolar couplings (and possibly, although less important, residual chemical shift anisotropy). In these solutions, the increase in polymer concentration leads to stronger intermolecular interactions and the molecular motions become restricted and slower. Under these conditions, residual magnetic dipolar couplings will be present causing the signals to broaden. The MAS spectrum shown supports the assumption that the broadening arises from anisotropic interactions rather than from a direct relation with the T_2 relaxation time. The magnetic dipolar interaction depends

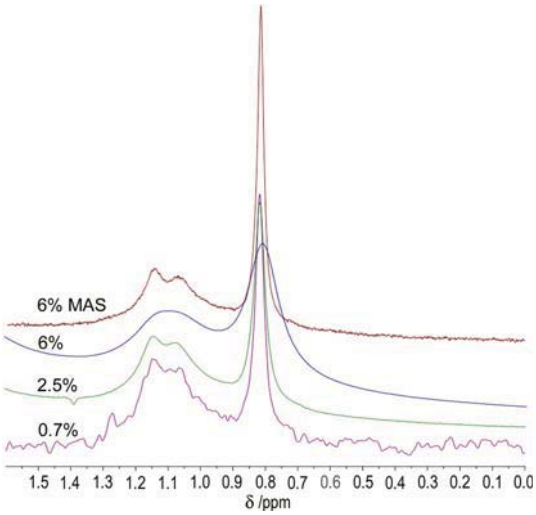

Figure 5. ^{2}H NMR spectra of PF8-d_{34} in toluene at indicated concentrations; the 6% MAS spectrum was acquired at 4 kHz spinning rate.

on the geometrical factor ($3\cos^2\theta-1$), where θ is the angle between the internuclear vector and the external magnetic field B_0. In nonviscous solutions the molecules undergo rapid and isotropic translational and rotational motion and the internuclear vectors are averaged over all orientations relative to B_0. In this situation ($3\cos^2\theta - 1$) becomes zero (the average of $\cos^2\theta$ over all directions is $^1/_3$) and the contribution of the dipolar interaction vanishes. MAS[61,62] NMR removes line broadening caused by dipolar interactions (and other anisotropic interactions such as chemical shift anisotropy and quadrupolar interaction) by averaging the orientation of all the internuclear vectors in the sample to an angle of 54.74° relative to B_0 by sample rotation at this so-called "magic" angle. This angle, $\theta = 54.74°$, is that for which ($3\cos^2\theta - 1$) becomes zero and the dipolar interaction vanishes. The line widths in the 6% MAS ^{1}H NMR spectra of PF8-d_{34} are comparable, or even narrower, than those in the 0.7% solution spectrum, showing that the line broadening is due to anisotropic interactions dependent on the ($3\cos^2\theta-1$) geometrical factor. These are due to the slower motion of the molecules in the concentrated solutions arising from the stronger polymer−polymer interactions through the alkyl side chains. The ^{2}H spectra obtained for the same solutions (Figure 5) allow the same conclusions. For the normal spectrum of the 6% solution we observe a loss of resolution which is regained in the MAS spectrum, indicating that anisotropic interactions, such as residual dipolar coupling and quadrupolar coupling, are the cause of line broadening in the concentrated solutions. Although the deuterated polymer has a higher molecular weight than the nondeuterated one, this does not seem to have any influence on the NMR spectral parameters.

Comparing the ^{1}H MAS NMR for the 6% solution and the ^{1}H spectra of the 0.7% solution, new resonances, at 0.97, 1.00, and 1.09 ppm, are detected in the former case. This finding is in agreement with the previous results in suggesting more rigid conformations of the alkyl chains in the 6% solution. A further, and as yet unattributed, broad signal is observed in the ^{1}H NMR spectrum of PF8-d_{34} around 1.35 ppm (Figure 4). Considering that we are looking at the residual proton signals for chain deuterated polymer, this may come from traces of defect or other impurity.

SANS. Polymer gels with spatial inhomogeneity are a materials class well studied by SANS, which is an ideal tool to probe the larger length scales of typical intermolecular distances, and thus complement our NMR measurements.

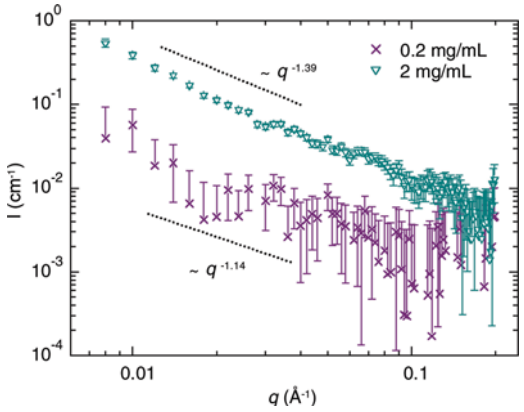

Figure 6. SANS data of PF8 in toluene-d_8 with concentrations 0.2 mg/mL (purple crosses) and 2 mg/mL (cyan down triangles). Dotted lines show the linear fits for comparison (shifted for clarity).

We have previously studied PF8 in a "good solvent", toluene, by SANS in moderate concentration (∼10 mg/mL)[30] and contrasted the results to the varying side chain length.[33] Chen and co-workers have conducted comprehensive studies of dilute (≤0.4 mg/mL)[38] PF8 toluene solutions by light scattering and dense toluene solutions (≥30 mg/mL)[31] by SANS. In the present work we extend such studies to the structural organization at larger sizes, by measuring at ultrasmall q ranges and scan over a broad range of polymer concentrations. Through this, we hope to achieve a more accurate idea of the larger length scale fluctuations unattainable by NMR.

Figure 6 plots the SANS data of PF8 in low-concentration (0.2−2 mg/mL) solution in toluene-d_8. Figure 7 plots the SANS data of the studied high-concentration samples (5−70 mg/mL) alongside the considered model fits. Structural parameters estimated from these fits are given in Table 3.

When the PF8 concentration is ≤10 mg/mL the curves decay as −1, indicative of dissolved rodlike polymers in the corresponding length scale (Figures 6 and 7). These data should be contrasted to the approximate length of the polymer that is ∼100 nm as calculated from the molecular weight and crystallographic length of the monomer (∼8.3 Å).[19] The persistence length l_p (∼10 nm) estimated from the Holtzer presentations for semidilute concentrations (Supporting Information) is consistent with the literature (8.6[18]−9.8 nm[38]) and thus corresponds to one-tenth of the polymer length. As l_p is much smaller than the polymer length, the polymer is expected to form Gaussian chains.

The overlap concentration (c^*),[63] where interpenetration of the polymer chains is assumed to begin, is approximated as $M_n/N_A(2R_g)^3 \approx 0.6$ mg/mL, where N_A is the Avogadro constant and where $R_g = 249$ Å is the radius of gyration measured for PF8 in dilute toluene solution at 25 °C.[38] Reference 38 gives R_g for a polymer with higher M_n than used in the present SANS measurement (128 kg/mol versus 47 kg/mol). However, c^* would not exceed 2 mg/mL if M_n was replaced by the higher value. As shown in Figure 6, both the data below (0.2 mg/mL) and above c^*(2 mg/mL) are similar except for a 10-fold difference in intensity. There seem to be a slight increase in decay from ∼−1.1 to ∼−1.4, which occurs for the samples with expected overlap of coils (∼2−10 mg/mL). The overlap becomes more apparent at very low q (∼0.006 Å^{-1}) where the data for 5−10 mg/mL samples shows few signs of leveling off, when exceeding the nominal length of individual polymers (Figure 7). An underestimation of the scatterer size is observed at the lowest q when the model of arbitrary shaped particles, expected polymer coils, is fitted to the data (orange lines in Figure 7).

When the PF8 concentration is ≥30 mg/mL, the data not only show an increase in intensity, but also a downturn at ~0.01 Å^{-1} and a significant upturn at < 0.01 Å^{-1} (Figure 7), which indicates an apparent phase transition. This effect is best seen when the data are normalized to the polymer concentration (Supporting Information). When the concentration is increased up to 70 mg/mL, the data begin to show two plateaus, one at ~0.03 Å^{-1} and another at ~0.001 Å^{-1}, pointing to the structure at two levels. As proposed in ref 31, the former effect is related to the polymer overlap and the latter arises from emerging aggregation or "segmental alignment" which is responsible for the network formation and gel appearance of the dense samples. The combination of Debye−Bueche and Ornstein−Zernike type scattering functions allows an estimation of the "blob" with the size ξ_d (~20 nm) representing the length scale where polymers appear separated. Accordingly, the data do not deviate much from −1 decay for $q > 0.01$ Å^{-1} and the calculated polymer diameter (~1 nm) corresponds to a single polymer chain for the length scales below ξ_d. This fluctuation does not yet lead to gelation but the network nodes emerge above this length scale. The model includes a larger length scale fluctuation with the size ξ_s (~60 nm) that is interpreted as a distance between the network nodes. The network nodes involve parts having a few chains forming ordered elongated bundles and the gel remains transparent. These aggregates are rather different from the compact quasi-two-dimensional aggregates found for poly(2,3-diphenyl-5-decyl-1,4-phenylenevinylene) (DP10-PPV) in toluene[34] or PF8 in the poorer solvent, methylcyclohexane.[15,26,27]

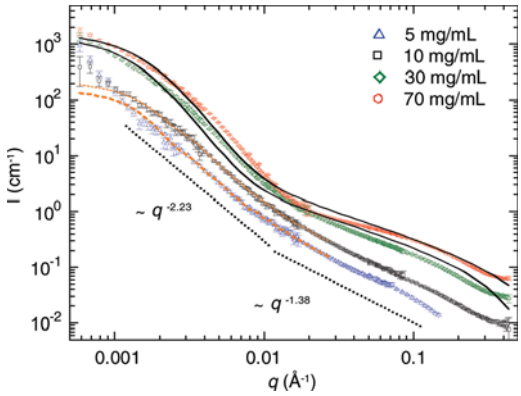

Figure 7. SANS data of PF8 in toluene-d_8 with concentrations 5 mg/mL (blue up triangles), 10 mg/mL (black squares), 30 mg/mL (green diamonds), and 70 mg/mL (red circles). Orange lines are fits to the arbitrary shaped particle "polymer coil" by software GNOM. Solid lines represent fits to the two-component model proposed in ref 31. Dotted black lines show the best linear fits for the case 10 mg/mL (shifted for clarity).

The idea of three-phase regimes and their approximate dimensions with increasing concentration are illustrated in Figure 8. At low concentrations, dissolved polymer coils with a persistence length l_p that is 1/10th of the polymer length, are observed, and may not have any contacts below c^*. The chains are forced to touch each others above c^*, and finally form a gel with the distance-ordered nodes separated by ξ_s. In this stage, the side chains are likely to be strongly interacting, in complete agreement with the NMR results in the present study. These results complement those shown by Chen and co-workers[31] for the following reasons. The low-concentration samples were not measured by SANS.[38] The previously reported q range for the high-concentration samples reached down to 0.003 Å^{-1} whereas our data extends this range down to 0.00058 Å^{-1}, showing us how the data level off at $q < 0.003$ Å^{-1} for $c \geq 30$ mg/mL. We, thus, complement these data and can be more confident with the estimated ξ_s value, while also obtaining the approximate size of scatterers corresponding to the very low q plateau (radius of gyration ~130 nm with the maximum dimension of ~300 nm). Moreover, our observation window reaches well beyond the total length of the polymer (~100 nm) and shows no clear Guinier plateau for $c \leq 10$ mg/mL (~0.001 Å^{-1}).

Some Comments on Solubility and Aggregation Behavior of PF8. In this study, both NMR and SANS show interchain interactions with PF8 upon increasing concentrations in toluene solution, and, together with semiempirical theoretical calculations, support the importance of side chain-side chain interactions in the aggregation behavior. This may help us provide more general guidelines on the aggregation of polyfluorenes in solutions. Polymer solution behavior is frequently treated by considering binary polymer−polymer, polymer−solvent and solvent−solvent interactions, through

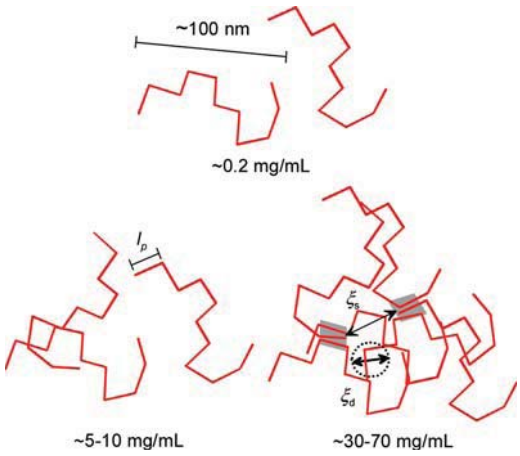

Figure 8. Idea of the intermolecular structure for PF8 in toluene-d_8 as a function of concentration. See text for details.

Table 3. Parameters Estimated from the Fits to the SANS data of PF8 in Toluene-d_8 [a]

	analyzed q range (Å^{-1})	concn = 0.2 mg/mL	concn = 2 mg/mL	concn = 5 mg/mL	concn = 10 mg/mL	concn = 30 mg/mL	concn = 70 mg/mL
α	0.00058−0.01	-	-	2.25 ± 0.02	2.21 ± 0.02	-	-
	0.0011−0.01	-	-	-	2.23 ± 0.02	-	-
	0.011−0.11	1.14 ± 0.11	1.39 ± 0.03	1.40 ± 0.01	1.38 ± 0.01	-	-
l_p (Å)	-	-	-	158 ± 26	127 ± 17	-	-
R_g (Å)	0.00058−0.027	-	-	1199 ± 36	1095 ± 34	-	-
D_{max} (Å)	-	-	-	~3250	~3250	-	-
ξ_s (Å)	0.00068−0.4	-	-	-	-	650 ± 9	550 ± 7
ξ_d (Å)	-	-	-	-	-	205 ± 30	206 ± 28
R (Å)	-	-	-	-	-	5. 0 ± 1.6	3.3 ± 1.6

[a] α and l_p stand for the scattering power for given q range and persistence length of an apparently stiff polymer. R_g and D_{max} represent radius of gyration and the maximum size of the scatterer. ξ_s, ξ_d, and R refer to the aggregate distance, mesh size and the polymer radius.

the Flory−Huggins[64−66] and Hildebrand-Scatchard[67−70] treatments. From the latter, and subsequent modifications,[70] a series of solubility parameters have been determined. Despite the simplicity of the approach, remarkable success has been achieved in predicting and interpreting various facets of the solution behavior of polymers. However, poly(9,9-dialkylfluorene)s belong to the family of "hairy-rod" polymers,[71,72] in which the relatively rigid backbone is surrounded by conformationally mobile side chains, and different interactions with solvent are anticipated for the backbone and side chains. Phenomenologically, the solution and phase behavior of polyfluorenes can be rationalized in terms of the nature of the solvent, the volume fraction of the polymer, the side chain size and shape and the molecular weight of the polymer.[13−17,30,33] In addition, experimental studies and molecular dynamics simulations on the anionic poly{1,4-phenylene-[9,9-bis(4-phenoxy-butylsulfonate)]fluorene-2,7-diyl} in mixed solvents strongly suggest specific solvent interactions with backbone, side chain and ionic regions of these systems.[73] Extension of these ideas to PF8 suggest that local solvation effects may also be important here, and that we need to consider separately the various pairwise interactions involving backbone, side chain and solvent.

Chlorinated alkanes are good solvents for polyfluorenes, and many other conjugated polymers. The fact that there is a reasonable attractive interaction with these solvents and the backbone is suggested by the monomer 2,7-dibromo-9,9-dioctylfluorene forming a solvated species on crystallization from chloroform.[74] As with interactions between many other aromatic molecules and halomethanes,[75] this probably involves an attractive contact charge transfer interaction. Since halomethanes and long-chain alkanes are generally completely miscible, there are no unfavorable solvent side-chain interactions, and polyfluorenes are dissolved in haloalkanes at the molecular level until very high polymer volume fractions.

If the solvent quality decreases, specific interactions involving the backbone or the side chains become important. One type of interaction which has frequently been invoked in aggregation behavior of aromatic molecules,[76] and applied to conjugated polymers, involves $\pi-\pi$ stacking. For example, Lazzaroni and colleagues[17] have suggested that $\pi-\pi$ stacking is responsible for formation of long fibrils of PF8 when it is deposited onto mica substrates from solution. However, from studies of the crystal structure of 9,9-di-*n*-octyl-9*H*-fluorene,[77] and other considerations,[35] the steric requirements of the alkyl groups at the 9-position strongly suggest that the backbones are prevented from coming close enough together for such $\pi-\pi$ stacking to occur in PF8. Further, a recent detailed critical analysis of the existence of $\pi-\pi$ stacking has been presented,[78] which recommends that instead of "stacking", these should be considered as $\pi-\pi$ interactions, which are only likely to be important in large unsaturated systems when they are spatially close. This is unlikely for interactions between two poly(9,9-dialkylfluorene) chains. From NMR data, there appears to be good evidence for $\pi-\pi$ interactions between the aromatic solvent toluene and polyfluorene backbones with PF8[31] and PF2/6.[35] These may involve a sandwich polymer−solvent−polymer association. However, these are still relatively weak attractions, and as we have shown in this paper from NMR spectral and relaxation data, with polymers having straight alkyl side chains, as in PF8, these are in competition with interactions between the alkyl chains, which, at high polymer concentration, may be one of the driving forces leading to gel formation. The process is dependent on van der Waals interactions between side chains on two different polymers. These increase with the chain length of the alkyl side chains.[79,80] In some cases, this may lead to β-phase formation.[40] These interactions are opposed by conformational disordering of the side chains,[80] and the observed phase behavior is a result of the subtle balance between these rather weak interactions. The differences in the phase behavior of poly(9,9-dialkylfluorene)s with different alkyl chain lengths in toluene solutions[33] are a consequence of this. With branched side chains, such as in PF2/6, van der Waals interactions between alkyl side chains are reduced, and there is little sign of β-phase formation.

In the case of poor solvents, such as tetrahydrofuran, cyclohexane, and methylcyclohexane,[24,26,40] there is little interaction between the solvent and the backbone, and the phase behavior is dominated by side chain interactions. Where straight alkyl chains are present, van der Waals interactions can favor stabilization of the β-phase. Further, for short alkyl chains these are unfavorable relative to backbone−backbone interactions, however for longer chains, the interactions are counterbalanced by alkyl chain disordering. We believe that this can explain the chain length dependence of β-phase formation,[81] with the optimum conditions occurring for the octyl side chain. In addition, because of the importance of van der Waals interactions, addition of other alkyl chain compounds, such as 1,8-diiodooctane[21] or phospholipids,[22] which can also interact with the PF8 side chains through van der Waals forces, can also stabilize the formation of the β-phase. There are suggestions that the β-phase in PF8 exists without aggregation.[23,82] In particular, single-molecule fluorescence microscopy has proved to be a powerful technique to study the conformational behavior of isolated chains of conjugated polymers,[83] and evidence has been presented for stress-induced β-phase formation in PF8 films.[82,84] Kinetic[24] and thermodynamic[40] arguments have also been presented that aggregation is not the driving force for β-phase formation. However, although β-phase formation may not require aggregation,[23,24,40] it is almost certainly stabilized by it, and we believe that the observation of interactions between the alkyl side chains of PF8 upon aggregation in toluene solutions supports the importance of their involvement in this. This is further supported from optical measurements as a function of alkyl chain length. For PF6, a spectral change with time is observed, going from a Gaussian-like absorption band to one with structure and more weighted to the red indicative of aggregation, but no beta phase can be induced, whereas for PF7 to PF9, this structured absorption band forms on thermal cycling and is also accompanied by beta phase formation. For PF10, the aggregate state does not seem to be stable but a small fraction of beta-phase formation can be induced.[81,85] In addition, for high-molecular-weight PF8, it is possible that β-phase formation for single molecules may result from backfolding of the longer chains leading to alkyl−alkyl interactions between chain ends.

V. Conclusions

NMR, SANS, and dynamic light scattering studies in this and previous works show that PF8 is present in dilute toluene solutions as isolated chains, but upon increasing polymer concentration, interchain interactions lead to association and, eventually, gel formation. As suggested by Chen and co-workers[31] this is likely to be associated, in part, with $\pi-\pi$ interactions involving toluene and the polymer backbone. However, interaction between alkyl side chains is also seen to play a major role in association and gel formation. This probably involves mainly van der Waals forces between the side chains, which will be strongly chain-length dependent. As has been suggested elsewhere based on the combination of classical molecular dynamics and DFT simulations

on model PF8 oligomers,[86] side-chain interactions play a major role in the association behavior of this class of polymers, and may be relevant to related areas, such as the stabilization of the β-phase in PF8.

Acknowledgment. The authors acknowledge the "Rede Nacional de RMN" for the spectrometer facilities, and Dr. Emeric Wasielewski for help in data acquisition. The Varian VNMRS 600 MHz spectrometer is part of the National NMR Network and was purchased in the framework of the National Programme for Scientific Re-equipment, contract REDE/1517/RMN/2005, with funds from POCI 2010 (FEDER) and "Fundação para a Ciência e a Tecnologia" (FCT). L.L.G.J. acknowledges FCT for the postdoctoral grant SFRH/BPD/26415/2006 and the "Laboratório de Computação Avançada", of the Department of Physics of the University of Coimbra, for the computing facilities (Milipeia Cluster). The experiments at ISIS (RB1010190) were supported by the European Commission under the seventh Framework Programme through the Key Action: Strengthening the European Research Area, Research Infrastructures. Contract No. CP-CSA_INFRA-2008-1.1.1 Number 226507-NMI3. We are grateful to Drs Sarah Rogers and Telma Costa for their assistance in these measurements, and to Professor Carlos F. G. C. Geraldes and a reviewer for valuable comments. M.K. and L.A. acknowledge ILL for economic support. L.A. is grateful for support from Adolphe Merkle Foundation, Fribourg.

Supporting Information Available: Figures showing SANS data of the high concentration samples normalized to the polymer concentration and the Holtzer plot of the same data.

References and Notes

(1) Sirringhaus, H.; Kawase, T.; Friend, R. H. *MRS Bull.* **2001**, *26*, 539–543.
(2) Voigt, M. M.; Guite, A.; Chung, D. Y.; Khan, R. U. A.; Campbell, A. J.; Bradley, D. D. C.; Meng, F. S.; Steinke, J. H. G.; Tierney, S.; McCulloch, I.; Penxten, H.; Lutsen, L.; Douheret, O.; Manca, J.; Brokmann, U.; Sonnichsen, K.; Hulsenberg, D.; Bock, W.; Barron, C.; Blankaert, N.; Springer, S.; Grupp, J.; Mosley, A. *Adv. Funct. Mater.* **2010**, *20*, 239–246.
(3) Grell, M.; Bradley, D. D. C. *Adv. Mater.* **1999**, *11*, 895–905.
(4) Nguyen, T. Q.; Yee, R. Y.; Schwartz, B. J. *J. Photochem. Photobiol. A: Chemistry* **2001**, *144*, 21–30.
(5) Banach, M. J.; Friend, R. H.; Sirringhaus, H. *Macromolecules* **2004**, *37*, 6079–6085.
(6) Neher, D. *Macromol. Rapid Commun.* **2001**, *22*, 1366–1385.
(7) Leclerc, M. *J. Polym. Sci. Part A: Polym. Chem.* **2001**, *39*, 2867–2873.
(8) Scherf, U.; List, E. J. W. *Adv. Mater.* **2002**, *14*, 477–487.
(9) Grimsdale, A. C.; Müllen, K. *Adv. Polym. Sci.* **2006**, *199*, 1–82.
(10) Abbel, R.; Schenning, A. P. H. J.; Meijer, E. W. *J. Polym. Sci. Part A: Polym. Chem.* **2009**, *47*, 4215–4233.
(11) Monkman, A.; Rothe, C.; King, S.; Dias, F. *Adv. Polym. Sci.* **2008**, *212*, 187–225.
(12) Knaapila, M.; Winokur, M. J. *Adv. Polym. Sci.* **2008**, *212*, 227–272.
(13) Knaapila, M.; Stepanyan, R.; Lyons, B. P.; Torkkeli, M.; Hase, T. P. A.; Serimaa, R.; Güntner, R.; Seeck, O. H.; Scherf, U.; Monkman, A. P. *Macromolecules* **2005**, *38*, 2744–2753.
(14) Byun, H. Y.; Chung, I. J.; Shim, H.-K.; Kim, C. Y. *Macromolecules* **2004**, *37*, 6945–6953.
(15) Knaapila, M.; Stepanyan, R.; Torkkeli, M.; Garamus, V. M.; Galbrecht, F.; Nehls, B. S.; Preis, E.; Scherf, U.; Monkman, A. P. *Phys. Rev. E* **2008**, *77*, 051803.
(16) Knaapila, M.; Stepanyan, R.; Lyons, B. P.; Torkkeli, M.; Monkman, A. P. *Adv. Funct. Mater.* **2006**, *16*, 599–609.
(17) Surin, M.; Hennebicq, E.; Ego, C.; Marsitzky, D.; Grimsdale, A. C.; Müllen, K.; Brédas, J.-L.; Lazzaroni, R.; Leclère, P. *Chem. Mater.* **2004**, *16*, 994–1001.
(18) Grell, M.; Bradley, D. D. C.; Long, X.; Chamberlin, T.; Inbasekaran, M.; Woo, E. P. *Acta Polym.* **1998**, *49*, 439–444.
(19) Grell, M.; Bradley, D. D. C.; Ungar, G.; Hill, J.; Whitehead, K. S. *Macromolecules* **1999**, *32*, 5810–5817.
(20) Teetsov, J.; Fox, M. A. *J. Mater. Chem.* **1999**, *9*, 2117–2122.
(21) Peet, J.; Brocker, E.; Xu, Y.; Bazan, G. C. *Adv. Mater.* **2008**, *20*, 1882–1885.
(22) Tapia, M. J.; Monteserín, M.; Burrows, H. D. *Abstracts XXIII IUPAC Symposium on Photochemistry*; Ferrara, Italy, July 11−16, 2010; abstract P296.
(23) Chunwaschirasiri, W.; Tanto, B.; Huber, D. L.; Winokur, M. J. *Phys. Rev. Lett.* **2005**, *94*, 107402.
(24) Dias, F. B.; Morgado, J.; Maçanita, A. L.; da Costa, F. P.; Burrows, H. D.; Monkman, A. P. *Macromolecules* **2006**, *39*, 5854–5864.
(25) Hickl, P.; Ballauff, M.; Scherf, U.; Müllen, K.; Lindner, P. *Macromolecules* **1997**, *30*, 273–279.
(26) Knaapila, M.; Dias, F. B.; Garamus, V. M.; Almásy, L.; Torkkeli, M.; Leppänen, K.; Galbrecht, F.; Preis, E.; Burrows, H. D.; Scherf, U.; Monkman, A. P. *Macromolecules* **2007**, *40*, 9398–9405.
(27) Chen, C.-Y.; Chang, C.-S.; Huang, S.-W.; Chen, J.-H.; Chen, H.-L.; Sum, C.-I.; Chen, S.-A. *Macromolecules* **2010**, *43*, 4346–4356.
(28) Fytas, G.; Nothofer, H. G.; Scherf, U.; Vlassopoulos, D.; Meier, G. *Macromolecules* **2002**, *35*, 481–488.
(29) Dias, F. B.; Knaapila, M.; Monkman, A. P.; Burrows, H. D. *Macromolecules* **2006**, *39*, 1598–1606.
(30) Knaapila, M.; Garamus, V. M.; Dias, F. B.; Almásy, L.; Galbrecht, F.; Charas, A.; Morgado, J.; Burrows, H. D.; Scherf, U.; Monkman, A. P. *Macromolecules* **2006**, *39*, 6505–6512.
(31) Rahman, M. H.; Chen, C.-Y.; Liao, S.-C.; Chen, H.-L.; Tsao, C.-S.; Chen, J.-H.; Liao, J.-L.; Ivanov, V. A.; Chen, S.-A. *Macromolecules* **2007**, *40*, 6572–6578.
(32) Burrows, H. D.; Knaapila, M.; Monkman, A. P.; Tapia, M. J.; Fonseca, S. M.; Ramos, M. L.; Pyckhout-Hintzen, W.; Pradhan, S.; Scherf, U. *J. Phys.: Condensed Matter* **2008**, *20*, 104210.
(33) Knaapila, M.; Almásy, L.; Garamus, V. M.; Ramos, M. L.; Justino, L. L. G.; Galbrecht, F.; Preis, E.; Scherf, U.; Burrows, H. D.; Monkman, A. P. *Polymer* **2008**, *49*, 2033–2038.
(34) Li, Y.-C.; Chen, C.-Y.; Chang, Y.-X.; Chuang, P.-Y.; Chen, J.-H.; Chen, H.-L.; Hsu, C.-S.; Ivanov, V. A.; Khalatur, P. G.; Chen, S.-A. *Langmuir* **2009**, *25*, 4668–4677.
(35) Rahman, M. H.; Liao, S.-C.; Chen, H.-L.; Chen, J.-H.; Ivanov, V. A.; Chu, P. P. J.; Chen, S.-A. *Langmuir* **2009**, *25*, 1667–1674.
(36) Somma, E.; Loppinet, B.; Chi, C.; Wegner, G. *Phys. Chem. Chem. Phys.* **2006**, *8*, 2773–2778.
(37) Ling, J.; Fomina, N.; Rasul, G.; Hogen-Esch, T. E. *J. Phys. Chem. B* **2008**, *112*, 10116–10122.
(38) Chen, J.-H.; Chang, C.-S.; Chang, Y.-X.; Chen, C.-Y.; Chen, H.-L.; Chen, S.-A. *Macromolecules* **2009**, *42*, 1306–1314.
(39) Justino, L. L. G.; Ramos, M. L.; Abreu, P. E.; Carvalho, R.; Sobral, A. J. F. N.; Scherf, U.; Burrows, H. D. *J. Phys. Chem. B* **2009**, *113*, 11808–11821.
(40) Kitts, C. C.; Vanden Bout, D. A. *Polymer* **2007**, *48*, 2322–2330.
(41) Traiphol, R.; Charoenthai, N.; Srikhirin, T.; Perahia, D. *Synth. Met.* **2010**, *160*, 1318–1324.
(42) Panyukov, S.; Rabin, Y. *Phys. Rep.* **1996**, *269*, 1–131.
(43) Shibayama, M. *Macromol. Chem. Phys.* **1998**, *199*, 1–30.
(44) Chen, S. H.; Su, A. C.; Chen, S. A. *J. Phys. Chem. B* **2005**, *109*, 10067–10072.
(45) Chen, S.-H.; Su, A.-C.; Chen, S.-A. *Macromolecules* **2006**, *39*, 9143–9149.
(46) Galbrecht, F.; Yang, X. H.; Nehls, B. S.; Neger, D.; Farrell, T.; Scherf, U. *Chem. Commun.* **2005**, *18*, 2378–2380.
(47) Heenan, R. K.; Penfold, J.; King, S. M. *J. Appl. Crystallogr.* **1997**, *30*, 1140–1147.
(48) Svergun, D. I. *J. Appl. Crystallogr.* **1992**, *25*, 495–503.
(49) Schmidt, M. W.; Baldridge, K. K.; Boatz, J. A.; Elbert, S. T.; Gordon, M. S.; Jensen, J. H.; Koseki, S.; Matsunaga, N.; Nguyen, K. A.; Su, S. J.; Windus, T. L.; Dupuis, M.; Montgomery, J. A. *J. Comput. Chem.* **1993**, *14*, 1347–1363.
(50) Becke, A. D. *J. Chem. Phys.* **1993**, *98*, 5648–5652.
(51) Lee, C.; Yang, W.; Parr, R. G. *Phys. Rev. B* **1988**, *37*, 785–789.
(52) Bylaska, E. J.; de Jong, W. A.; Govind, N.; Kowalski, K.; Straatsma, T. P.; Valiev, M.; Wang, D.; Apra, E.; Windus, T. L.; Hammond, J.; Nichols, P.; Hirata, S.; Hackler, M. T.; Zhao, Y.; Fan, P.-D.; Harrison, R. J.; Dupuis, M.; Smith, D. M. A.; Nieplocha, J., Tipparaju, V.; Krishnan, M.; Wu, Q.; Van Voorhis, T.; Auer, A. A.; Nooijen, M.; Brown, E.; Cisneros, G.; Fann, G. I.; Fruchtl, H.; Garza, J.; Hirao, K.; Kendall, R.; Nichols, J. A.; Tsemekhman, K.; Wolinski, K.; Anchell, J.; Bernholdt, D.; Borowski, P.; Clark, T.; Clerc, D.; Dachsel, H.; Deegan, M.; Dyall, K.; Elwood, D.; Glendening, E.; Gutowski, M.; Hess, A.; Jaffe, J.; Johnson, B.; Ju,

J.; Kobayashi, R.; Kutteh, R.; Lin, Z.; Littlefield, R.; Long, X.; Meng, B.; Nakajima, T.; Niu, S.; Pollack, L.; Rosing, M.; Sandrone, G.; Stave, M.; Taylor, H.; Thomas, G.; van Lenthe, J.; Wong, A. Zhang, Z. NWChem, A Computational Chemistry Package for Parallel Computers, Version 5.1; Pacific Northwest National Laboratory: Richland, WA, 2007.High Performance Computational Chemistry: An Overview of NWChem a Distributed Parallel Application. Kendall, R. A.; Apra, E.; Bernholdt, D. E.; Bylaska, E. J.; Dupuis, M.; Fann, G. I.; Harrison, R. J.; Ju, J.; Nichols, J. A.; Nieplocha, J.; Straatsma, T. P.; Windus, T. L.; Wong, A. T. *Comput. Phys. Commun.* **2000**, *128*, 260–283.
(53) Stewart, J. J. P. *J. Mol. Modeling* **2007**, *13*, 1173–1213.
(54) MOPAC2007, James J. P. Stewart, Stewart Computational Chemistry, Version 8.087L web: HTTP://OpenMOPAC.net.
(55) Ranger, M.; Rondeau, D.; Leclerc, M. *Macromolecules* **1997**, *30*, 7686–7691.
(56) Bloembergen, N.; Purcell, E. M.; Pound, R. V. *Phys. Rev.* **1948**, *73*, 679–712.
(57) Gil, V. M. S.; Geraldes, C. F. G. C. *Ressonância Magnética Nuclear, Fundamentos, Métodos w Aplicações*, 2nd ed.; Fundação Calouste Gulbenkian: Lisbon, 2002.
(58) Heatley, F. *Prog. Nucl. Magn. Reson. Spectrosc.* **1979**, *13*, 47–85.
(59) (a) Lipari, G.; Szabo, A. *J. Am. Chem. Soc.* **1982**, *104*, 4546–4559. (b) Lipari, G.; Szabo, A. *J. Am. Chem. Soc.* **1982**, *104*, 4559–4570.
(60) Ayalur-Karunakaran, S.; Blumich, B.; Stapf, S. *Langmuir* **2009**, *25*, 12208–12216.
(61) (a) Andrew, E. R.; Bradbury, A.; Eades, R. G. *Nature* **1959**, *183*, 1802–1803. (b) Andrew, E. R.; Szczesniak, E. *Prog. Nucl. Magn. Reson. Spectrosc.* **1995**, *28*, 11–36.
(62) Lowe, I. J. *Phys. Rev. Lett.* **1959**, *2*, 285–287.
(63) Ying, Q.; Chu, B. *Macromolecules* **1987**, *20*, 362–366.
(64) Huggins, M. L. *J. Chem. Phys.* **1941**, *9*, 440.
(65) Flory, P. J. *J. Chem. Phys.* **1941**, *9*, 660–661.
(66) Flory, P. J. *Principles of Polymer Chemistry*: Cornell University Press: Ithaca, NY, 1953.
(67) Hildebrand, J. H.; Scott, R. L. *Solubility of Non-Electrolytes*, 3rd ed.; Reinhold: New York, 1950.
(68) Hildebrand, J. H.; Prausnitz, J. M.; Scott, R. L. *Regular and Related Solutions*; Van Nostrand-Reinhold: Princeton, NJ, 1970.
(69) Scatchard, G. *Chem. Rev.* **1949**, *44*, 7–35.
(70) Barton, A. F. M. *Chem. Rev.* **1975**, *75*, 731–753.
(71) Wegner, G. *Macromol. Chem. Phys.* **2003**, *204*, 347–357.
(72) Subbotin, A.; Stepanyan, R.; Knaapila, M.; Ikkala, O.; ten Brinke, G. *Eur. Phys. J. E* **2003**, *12*, 333–345.
(73) Burrows, H. D.; Fonseca, S. M.; Silva, C. L.; Pais, A. A. C. C.; Tapia, M. J.; Pradhan, S.; Scherf, U. *Phys. Chem. Chem. Phys.* **2008**, *10*, 4420–4428.
(74) Leclerc, M.; Ranger, M.; Bélanger-Gariépy, F. *Acta Crystallogr., Sect. C* **1998**, *C54*, 799–801.
(75) Davis, K. M. C.; Farmer, M. F. *J. Chem. Soc. B* **1968**, 859–862.
(76) Hunter, C. A.; Lawson, K. R.; Perkins, J.; Urch, C. J. *J. Chem. Soc., Perkin Trans. 2* **2001**, 651–669.
(77) McFarlane, S.; McDonald, R.; Veinot, J. G. C. *Acta Crystallogr. C* **2005**, *C61*, O671–O673.
(78) Grimme, S. *Angew. Chem., Int. Ed.* **2008**, *47*, 3430–3434.
(79) Nagle, J. F.; Goldstein, M. *Macromolecules* **1985**, *18*, 2643–2652.
(80) Bazuin, C. G.; Guillon, D.; Skoulios, A.; Amorim da Costa, A. M.; Burrows, H. D.; Geraldes, C. F. G. C.; Teixeira-Dias, J. J. C.; Blackmore, E.; Tiddy, G. J. T. *Liq. Cryst.* **1988**, *3*, 1655–1670.
(81) Bright, D.; Dias, F. B.; Galbrecht, F.; Scherf, U.; Monkman, A. P. *Adv. Funct. Mater.* **2009**, *19*, 67–73.
(82) Da Como, E.; Becker, K.; Lupton, J. M. *Adv. Polym. Sci.* **2008**, *212*, 293–318.
(83) Lammi, R. K.; Barbara, P. F. *Photochem. Photobiol. Sci.* **2005**, *4*, 95–99.
(84) Da Como, E.; Becker, K.; Feldman, J.; Lupton, J. M. *Nano Lett.* **2007**, *7*, 2993–2998.
(85) Bright, D. W.; Galbrecht, F.; Scherf, U.; Monkman, A. P. *Macromolecules* **2010**, *43*, 7860–7863.
(86) Kilina, S.; Batista, E. R.; Yang, P.; Tretiak, S.; Saxena, A.; Martin, R. L.; Smith, D. L. *ACS Nano* **2008**, *2*, 1381–1388.